High sensitivity face shear magneto-electric composite array for weak magnetic field sensing

Yun Lu
yl544@uowmail.edu.au

Zhenxiang Cheng
University of Wollongong, cheng@uow.edu.au

Jianguo Chen

Weihua Li
University of Wollongong, weihuali@uow.edu.au

Shujun Zhang
University of Wollongong, shujun@uow.edu.au

Recommended Citation

High sensitivity face shear magneto-electric composite array for weak magnetic field sensing

Abstract

© 2020 Author(s). A magnetic field sensor is designed and fabricated using a piezoelectric face shear mode Pb(Mg1/3Nb2/3)O3-PbTiO3 (PMN-PT)/Metglas magneto-electric (ME) composite. An outstanding ME coupling coefficient up to 1600 V/(cm Oe) was experimentally achieved, being ∼50% higher than the value from the extensional PMN-PT/Metglas ME composite with the same volume. The detection limit was found to be 2 × 10-6 Oe for the DC magnetic field, while it was 2 × 10-8 Oe for the AC magnetic field. The sensitivity of the face shear mode PMN-PT/Metglas ME composite is about one order of magnitude higher than that of a 32 extensional mode PMN-PT/Metglas based ME composite in sensing a weak DC magnetic field. A sensing array was also designed based on the ME composite to image weak DC magnetic fields, demonstrating a great potential promising for sensing weak magnetic fields.

Disciplines

Engineering | Science and Technology Studies

Publication Details

High sensitivity face shear magneto-electric composite array for weak magnetic field sensing

Yun Lu (iD), Zhenxiang Cheng (iD), Jianguo Chen (iD), Weihua Li (iD), and Shujun Zhang (iD)

View Online   Export Citation   CrossMark

ARTICLES YOU MAY BE INTERESTED IN

High sensitivity face shear magneto-electric composite array for weak magnetic field sensing

View Online   Export Citation   CrossMark

Yun Lu,[1] Zhenxiang Cheng,[1] Jianguo Chen,[2] Weihua Li,[3] and Shujun Zhang[1,a]

AFFILIATIONS

[1]Institute for Superconducting and Electronic Materials, Australian Institute of Innovative Materials, University of Wollongong, Wollongong, NSW 2500, Australia
[2]School of Materials Science and Engineering, Shanghai University, Shanghai 200444, People's Republic of China
[3]School of Mechanical, Materials and Mechatronic Engineering, University of Wollongong, Wollongong, NSW 2522, Australia

[a]Author to whom correspondence should be addressed: shujun@uow.edu.au

ABSTRACT

A magnetic field sensor is designed and fabricated using a piezoelectric face shear mode $Pb(Mg_{1/3}Nb_{2/3})O_3–PbTiO_3$ (PMN–PT)/Metglas magneto-electric (ME) composite. An outstanding ME coupling coefficient up to 1600 V/(cm Oe) was experimentally achieved, being ∼50% higher than the value from the extensional PMN–PT/Metglas ME composite with the same volume. The detection limit was found to be 2×10^{-6} Oe for the DC magnetic field, while it was 2×10^{-8} Oe for the AC magnetic field. The sensitivity of the face shear mode PMN–PT/Metglas ME composite is about one order of magnitude higher than that of a 32 extensional mode PMN–PT/Metglas based ME composite in sensing a weak DC magnetic field. A sensing array was also designed based on the ME composite to image weak DC magnetic fields, demonstrating a great potential promising for sensing weak magnetic fields.

Published under license by AIP Publishing. https://doi.org/10.1063/5.0011931

I. INTRODUCTION

Magnetoelectric (ME) coupling devices have been actively studied for potential tools as weak magnetic field sensors, as alternatives to low-sensitivity Hall-base magnetometers, and expensive superconducting quantum interference devices (SQUIDs), for example, bio-magnetic sensing,[1,2] where the sensitivity is a key challenge. Although SQUIDs can be used for weak magnetic field measurements, they require liquid helium cooling with obvious disadvantages in terms of cost, temperature isolation, and a considerable amount of energy during the operation.

Magnetic sensors in the form of composites with laminated piezomagnetic (PM)/piezoelectric (PE) layers have recently reported to possess many advantages due to their excellent magnetoelectric coupling characteristics, high sensitivity, and wide operating temperature range.[3,4] In addition, the 2–2 layer-structured ME composite exhibits a low equivalent noise level of ∼1 pT/Hz$^{1/2}$ in an AC magnetic field of 1 kHz.[5] The ability to sense a weak magnetic field is as low as 8×10^{-6} Oe,[6] in stark contrast to the value of 3.5×10^{-2} Oe achieved by a commercially available Hall effect magnetometer.[7] Due to the low piezoelectric coefficient in many piezoelectric materials, however, the ME composite could only provide limited sensing resolution, which limited its ability to sense weak magnetic fields.

Compared to ferroelectric polycrystalline ceramics, the $Pb(Mg_{1/3}Nb_{2/3})O_3–PbTiO_3$ (PMN–PT) relaxor ferroelectric single crystal provides outstanding PE characteristics [piezoelectric charge coefficient, $d_{32} \approx -1200$ pC/N vs $d_{31} \approx 300$ pC/N in lead zirconate titanate (PZT) ceramics].[8,9] The ME composite based on mechanically coupled PMN–PT and Metglas shows a remarkable enhancement in its capability to convert a magnetic field into electric signals.[10] A longitudinally magnetized, transversely poled (L-T) PMN–PT/Metglas composite was found to have a ME coupling coefficient as large as 1100 V/(cm Oe) at its resonant frequency.[11] The highest piezoelectric charge coefficient of 3000 pC/N has been reported in the thickness shear mode of PMN–PT;[12] however, its low mechanical quality factor (Q_m of 20–30)[13] will lead to a high mechanical loss,[14] which greatly limits its ME coupling performance.

It is interesting to note that the face shear mode can be achieved in a Zt ±45° cut [011] oriented PMN–PT single crystal, possessing high piezoelectric charge coefficients (d_{36} of up to 1700 pC/N)[15] and a good mechanical quality factor ($Q_m \geq 120$),[16] thus attracting extensive attentions for actuator,[17] sensor,[18] and

motor applications.[19–21] Recently, an ME sensor based on a face shear mode Pb(Mg$_{1/3}$Nb$_{2/3}$)O$_3$–Pb(ZrTi)O$_3$ (PMN–PZT)/Metglas composite sensor was recently reported to possess outstanding sensitivity to AC magnetic fields.[22] However, the potential sensing capability of the face shear mode ME sensor to both AC and DC magnetic fields needs further comprehensive investigation, where the anisotropic characteristic and its application have not been reported.

In this research, we systematically study the property of the face shear PMN–PT/Metglas ME composite. The sensitivity and ME coupling property were theoretically calculated and experimentally confirmed. Then, an ME sensor array was designed and fabricated using the proposed face shear mode PMN–PT/Metglas ME composite. The ME composite array is able to determine the accurate spatial location of a weak static magnetic field, by using the anisotropic property of the ME composite. This work suggests great potential of our piezoelectric ME composite array design for sensing of weak magnetic signals, in both DC and AC magnetic fields.

II. EXPERIMENTAL SETUP

To prepare the face shear ME composite, the PMN–PT single crystal sample was prepared by rotating at a 45° angle along the z axis [011] direction, cutting into a square-shaped plate with dimensions of $10 \times 10 \times 0.5$ mm^3, as shown in Fig. 1(a). The specifically designed dimensions were to ensure that the crystal could operate in the 36-face shear mode to utilize its outstanding piezoelectric properties.[15] Silver electrodes were deposited on the two [011] surfaces, and then the crystal was poled at the electric field of 10 kV/cm at room temperature. The poled PMN–PT single crystal was bound with Metglas foil (2605SA1) using an electrically conducting epoxy (MG Chemicals silver conductive epoxy adhesive 8330) and then cured for 24 h at room temperature. The impedance spectrum of the fabricated ME composite was characterized using an impedance analyzer (HP4294A, Agilent Technologies Inc.). The ME composite, shield, and solenoid coil were integrated into the sensing element as shown in Fig. 1(b). The ME composite was placed in the nonmagnetic non-conducting shield to isolate it from the electric noise of the environment. A solenoid coil was employed to generate an AC magnetic field. When the AC magnetic field alternately changes along the diagonal direction of the composite, the Metglas foil will generate in-plane displacement in the PMN–PT crystal to move along the AC magnetic field, leading to in-plane displacement, from which electric charge will be induced on the two surfaces of the PMN–PT crystal based on the piezoelectric effect.[23,24] The output AC voltage signal is measured by a lock-in amplifier (SR 830, Stanford Research).

III. RESULTS AND DISCUSSION

A. Operation mode and the calculated equivalent magnetic noise density (EMND)

Figure 1(c) shows a measured impedance spectrum of the ME composite operating in the free vibration mode over the frequency range of 40 Hz–120 kHz at room temperature. The resonant frequency and anti-resonant frequency were found to be 85 kHz

and 107 kHz, respectively. For a rectangular shaped composite, the resonant frequency can be evaluated by[15]

$$f_r = \frac{F}{a+b} \sqrt{\frac{1}{\bar{\rho} \cdot \bar{s}}}, \tag{1}$$

where $F \sim 1.28$ is a correction constant, a is the length and b the width of the composite, $\bar{\rho} \sim 8$ g/cm^3 is the equivalent density of the composite, and $\bar{s} \sim 65$ pm^2/N is the equivalent elastic compliance of the composite, which can be estimated by[25]

$$\frac{1}{\bar{s}} = \left[\frac{n_c}{s_c} + \frac{n_l}{s_l} \right], \tag{2}$$

where n_c and n_l are the volume ratios of the crystal and load components (epoxy and Metglas), respectively, and s_c and s_l are the elastic compliance values of the crystal and load components (epoxy and Metglas), respectively. For the proposed design, the calculated resonant frequency is 87 kHz, which is very close to the measured value of 85 kHz. The minor difference is attributed to the composite fabrication process and the error in calculating the equivalent parameters. The dielectric loss tangents tan (δ) is found to be ~1.6% due to the epoxy adhesive, while the mechanical quality factor of the composite can be evaluated by $Q = f_r/\Delta f$, which is found to be ~110. The details of parameters of the composite are given in Table I.

The theoretical sensitivity of the fabricated sensor can be evaluated by determination of the equivalent magnetic noise density (EMND),[26] which consists of the dielectric loss noise and the impedance thermal noise, and it can be calculated from the following equation:[27,28]

$$\text{EMND} = \frac{\sqrt{\dfrac{4 \cdot k \cdot T \cdot C_p \cdot \tan\delta}{2 \cdot \pi \cdot f}} + \sqrt{\dfrac{4 \cdot k \cdot T}{(2 \cdot \pi \cdot f)^2 \cdot Z'}}}{t_p \cdot \alpha_{ME}}, \tag{3}$$

where $\sqrt{\frac{4 \cdot k \cdot T \cdot C_p \cdot \tan\delta}{2 \cdot \pi \cdot f}}$ is the dielectric loss noise, $\sqrt{\frac{4 \cdot k \cdot T}{(2 \cdot \pi \cdot f)^2 \cdot Z'}}$ is the impedance thermal noise, and t_p and α_{ME} represent the thickness of the crystal and the ME coupling coefficient, respectively. For the noise due to the dielectric loss $\sqrt{\frac{4 \cdot k \cdot T \cdot C_p \cdot \tan\delta}{2 \cdot \pi \cdot f}}$, where k, T, C_p, tan (δ), and f represent Boltzmann's constant, the temperature in kelvin, the capacitance of the composite, the dielectric loss, and the frequency, respectively. For the impedance thermal noise $\sqrt{\frac{4 \cdot k \cdot T}{(2 \cdot \pi \cdot f)^2 \cdot Z'}}$, Z' is the real part of the impedance. EMND was calculated based on the measured impedance as function of frequency at room temperature, where the measurement was performed in the grounded noise isolation box to avoid external electromagnetic noise. Figure 1(d) displays the calculated EMND curve of the ME composite. The corresponding magnetic noise density is found to be 0.1 pT/Hz$^{1/2}$ at the antiresonant frequency of 107 kHz, which is much improved compared to the resolution of the reported ME magnetic field sensor (0.5 pT/Hz$^{1/2}$).[29] The low EMND allows the fabricated ME sensor to give a clear signal at a weak magnetic field, contributing to the improved sensitivity of the device.
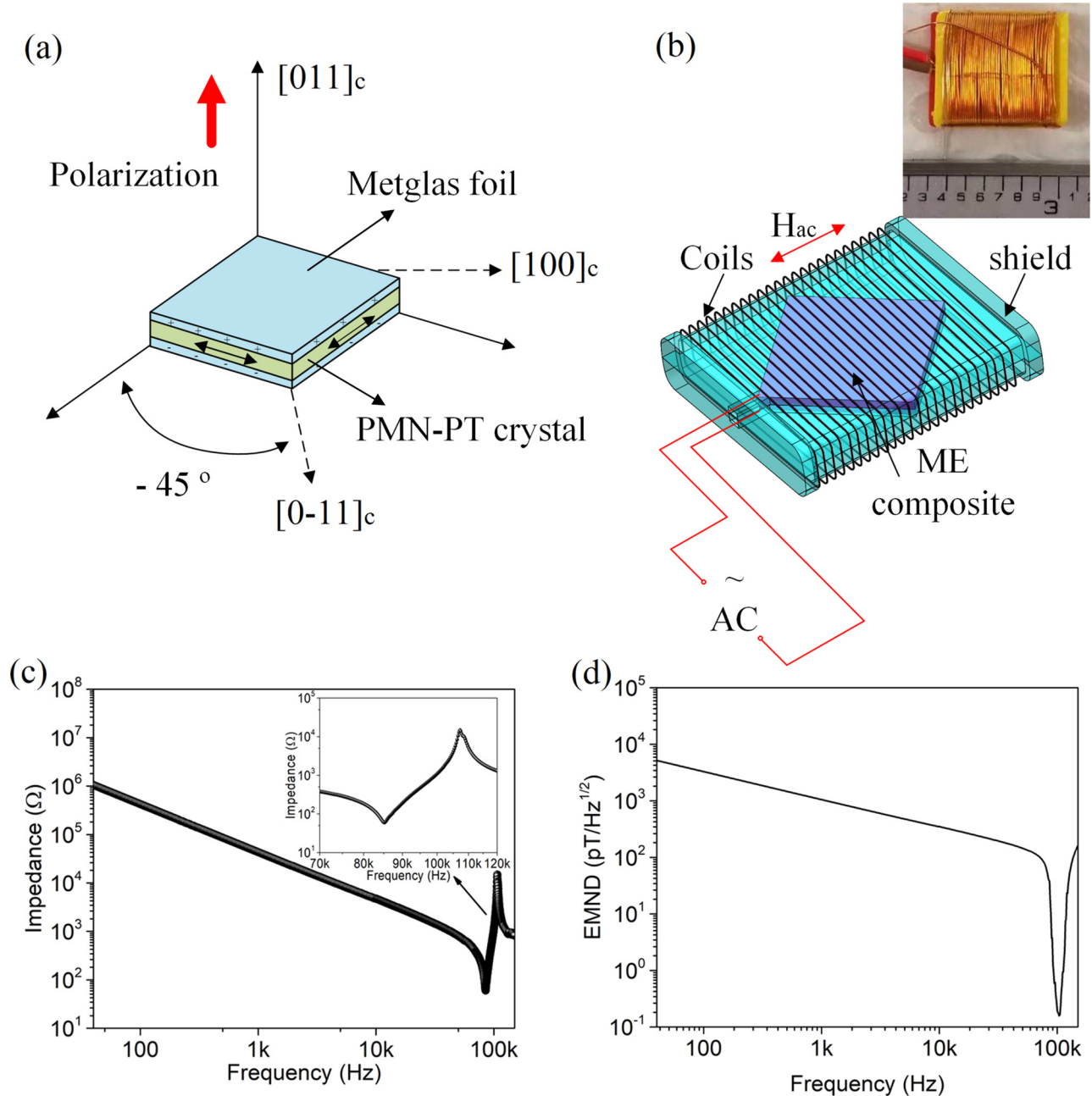
FIG. 1. (a) Schematic view and operation principle of the face shear mode ME composite. (b) Schematic view and photograph of the sensing element. (c) Impedance spectrum of the face shear PMN–PT/Metglas composite, with enlargement in the inset. (d) Calculated equivalent magnetic noise density (EMND) of the magnetic field sensor.

B. ME coupling properties of the face shear mode ME composite

The ME coupling property at the off resonant condition is tested at a quasi-static frequency of 1 kHz. The magnetic field is generated by Helmholtz coils. The detailed parameter of the

Helmholtz coils is listed in Table II. Figure 2(a) shows that the room temperature ME response depends on the DC magnetic field with the AC magnetic field fixed at H_{ac} of 0.1 Oe (1 kHz). The output AC voltage shows a near-linear increase with an increasing DC bias magnetic field up to 6 Oe. The maximum output voltage

TABLE I. Parameter details of the face shear mode PMN–PT/Metglas ME composite.

Parameters	Length (mm)	Width (mm)	Thickness (mm)	f_r (Hz)	f_a (Hz)	d_{36} (pC/N)	tan (δ) (%)	Q
	10	10	0.61	85 220	107 160	1700	1.6	110

of ~30 mV (1 kHz) was acquired at H_{dc} of 6 Oe. The equivalent ME coupling coefficient was calculated by $\alpha_{ME} = \frac{\partial E}{\partial H}$,[23,30–33] leading to the maximum quasi-static α_{ME} being on the order of ~6 V/(cm Oe). From this experiment, it is obvious that the intensity of the DC magnetic field can be measured by the generated voltage in the ME composite. The ME coupling coefficient tends to decrease at higher magnetic field, due to the magnetostriction of the Metglas as it approaches saturation.[34] The inset gives the first derivative of the α_{ME}, which is calculated by $D_{ME} = \Delta\alpha_{ME}/\Delta H$. Note that the maximum D_{ME} and the maximum voltage are not simultaneously achieved at the same magnetic field. In this case, the maximum D_{ME} is acquired at the DC magnetic field of H_{dc} = 2.2 Oe. This can be attributed to the increase of magnetic saturation in the Metglas foil under a DC magnetic field larger than 2.2 Oe.

The dynamic ME coefficient was measured as a function of excitation frequency under the fixed DC bias magnetic field, H_{dc} = 6 Oe. As shown in Fig. 2(b), a giant ME coupling coefficient calculated based on $\alpha_{ME} = \frac{\partial E}{\partial H}$ was found to be ~1600 V/(cm Oe) at the anti-resonant frequency of 107.6 kHz, which is ~50% higher than that reported for a 32 extensional mode PMN–PT based ME composite with the same volume.[11] The enhancement of the ME coupling coefficient is attributed to the improved piezoelectric charge coefficient (d_{36} ~ 1700 pC/N vs d_{32} ~ 1200 pC/N) and mechanical quality factor for the face shear mode.

C. Anisotropic characteristic of the ME composite and the magnetic sensitivity

In order to determine the sensitivity of the ME sensor, the voltage output of the $10 \times 10 \times 0.5$ mm³ face shear PMN–PT/Metglas ME composite was measured under different amplitudes of AC and DC magnetic fields at its anti-resonant frequency. Figure 3(a) displays the measured AC voltage as a function of H_{ac} with a DC magnetic field H_{dc} = 6 Oe. Note that the magnetic field sensor exhibits a clear ME response to a weak AC magnetic field as low as 2×10^{-8} Oe at an anti-resonant frequency of 107.6 kHz with the ME voltage output being on the order of ~4.5 μV. The detection limit 2×10^{-8} Oe of the studied sensor is much improved than the reported ME composite sensor (9.2×10^{-8} Oe).[35] The voltage output increases linearly as the AC magnetic field increases with a slope of ~80 V/Oe. The calculated ME coupling coefficient is found to be ~1600 V/(cm Oe), which is in a good agreement with the measured dynamic ME coupling coefficient. Figure 3(b)

presents the ME voltage as a function of time in a step-change H_{ac} from 0 (noise) to 2×10^{-7} Oe at frequency of 107.6 kHz. A noise of ~2 μV was measured at the frequency of 107.6 kHz. This noise is attributed to the combination of the impedance noise, thermal noise from the ME composite, and the noise from the lock-in amplifier and electric circuit. The experimental result shows a good repeatable output in response to the AC magnetic field. All these results demonstrate that the studied magnetic field sensor possesses a high sensitivity to weak AC magnetic fields with high reliability. Furthermore, the feasibility of calibrating a weak AC magnetic field via the output AC voltage of the sensor can be experimentally proved.

Figure 3(c) shows the maximum voltage output vs the angle between the x and y directions at H_{dc} = 6 Oe. The maximum output is found to be about 30 mV when the rotation angle reached 50° and 225°, respectively. Meanwhile, the minimum voltage is found to be ~8 mV at 120° and 315°, respectively, showing a strong anisotropic characteristic. This result agrees with the anisotropic behavior of the face shear piezoelectric constant d_{36} of the PMN–PT crystal.[36] Therefore, the relative position between the DC magnetic target and the sensor can be monitored by measuring the output AC voltage. Figure 3(d) displays the ME coupling property under a weak DC magnetic field. The detection limit is about 2×10^{-6} Oe, which is much improved over that reported for an ultra-sensitive ME sensor, being on the order of 8×10^{-6} Oe.[6] Clearly, the calculated response of the ME sensor to a weak H_{dc} field is found to be ~1 V/Oe at $H_{dc} \leq 1 \times 10^{-4}$ Oe, being decreased to ~5 mV/Oe for H_{dc} = 6 Oe due to the magnetization saturation of Metglas at elevated H_{dc}.

D. Magnet target sensing using the sensing array

Sensing the position of a magnet target is one of the applications of the ME composite.[37–40] To achieve the accurate position of the magnetic field source, one of the challenges is to isolate unwanted noise from the original output AC signal. To solve this problem, a sensing array was developed based on the ME composite. To build the sensing array, a total 43 pieces of the face shear mode PMN–PT/Metglas ME sensing elements were arrayed in a line as shown in Fig. 4(a). A permanent magnet with dimensions of $10 \times 10 \times 30$ mm³ was used as a target. Figure 4(b) displays the simulated distribution of the magnetic flux around the magnet and the sensor array. Because of the relative positions of the array and the magnet, the angle between the magnetic flux from the magnet and each sensing element is different. A lock-in amplifier (SR 830) was used to measure the output voltage from each sensing element and then the output results were built into a 1D voltage curve. The small difference in the angle is reflected in the output voltage curve of the array due to the anisotropic nature of the device. By processing the voltage curve, the contribution of the magnetic field
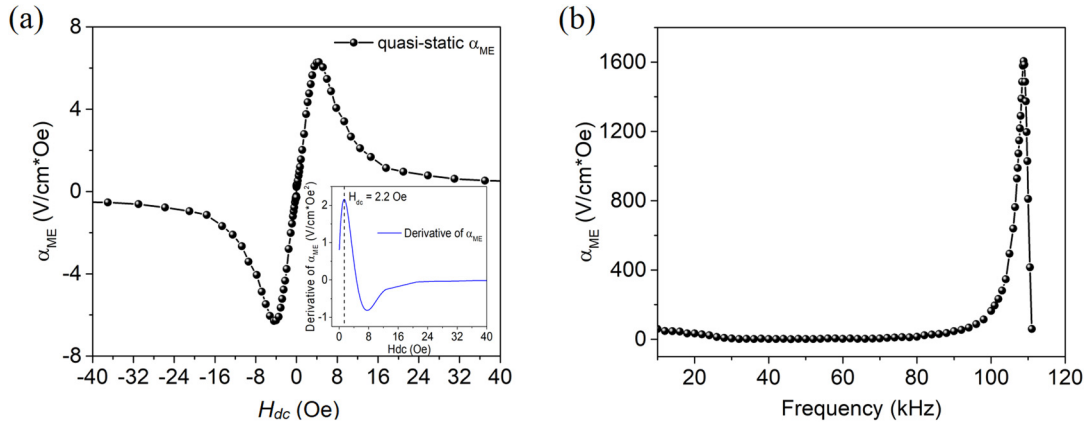
TABLE II. Parameter of the Helmholtz coils.

Parameter	Diameter (mm)	Turns	Max I (A)	Resistance (Ω)
	70	30	3	5

FIG. 2. ME coupling property of the ME composite sensor. (a) Measured quasi-static direct ME coefficient as a function of the magnetic bias H_{dc} at the AC magnetic field $H_{ac} = 0.1$ Oe (1 kHz), while the first derivative of α_{ME} is given in the inset. (b) Measured ME coupling coefficient as a function of frequency at the optimal DC magnetic field of 6 Oe.
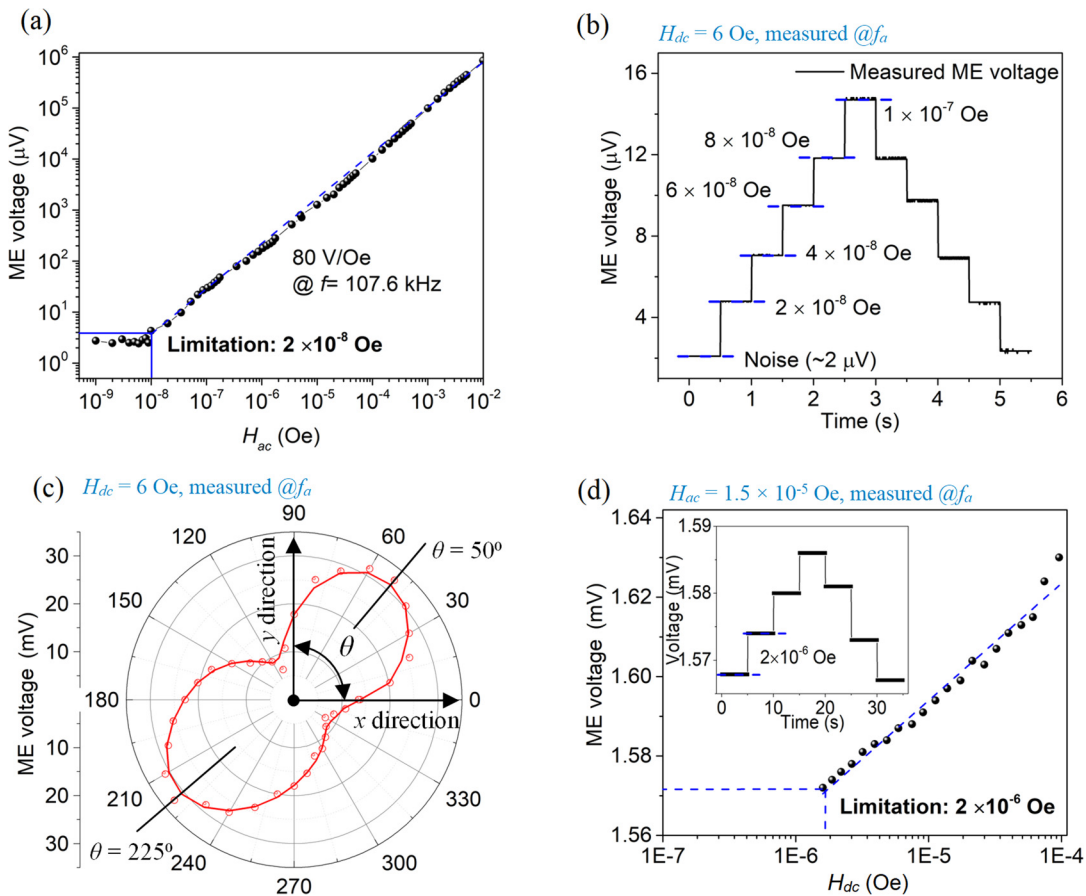
FIG. 3. AC magnetic field sensing. (a) Determination of the detection limit for the AC magnetic field and ME voltage output of the magnetic field sensor as a function of AC magnetic fields. (b) Step-change measurement of the magnetic sensitivity to a small range of AC magnetic field from 2×10^{-8} Oe to 1×10^{-7} Oe. (c) The ME response depends on the angle between the x direction (i.e., [0–11] direction of the crystal) and the y direction (direction of the DC magnetic field). (d) The detection limit for the DC magnetic field, with a step-change test of the output voltage as a function of time under different DC magnetic fields given in the inset.

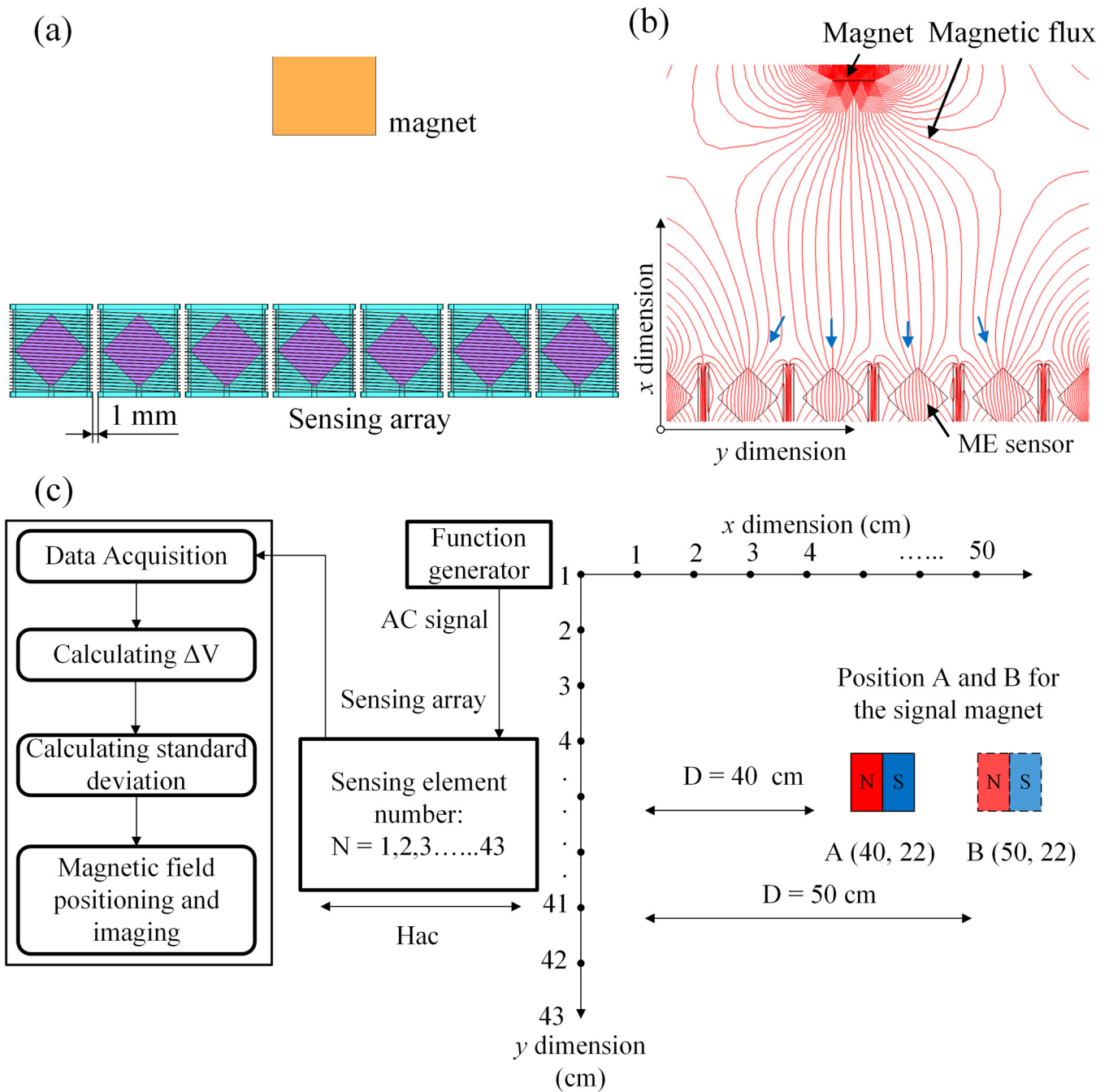**FIG. 4.** (a) Schematic view of the sensing array. (b) Simulated magnetic flux distribution in the sensing array. (c) The process of magnetic field positioning and imaging.

intensity can be isolated, and the real position of the magnet target can be confirmed.

To generate a weak magnetic field, the target magnet was placed at the A (40, 22) and B (50, 22) positions, as shown in Fig. 4(c). The numbers 40 and 22 of the (40, 22) coordinate represent the distances between the sensing array and the magnet target along the x axis and y axis in centimeters, respectively. By using the finite element analysis model, the magnetic field was found to be on the order of 10^{-5} Oe and 10^{-6} Oe at the A and B positions, respectively. The difference in output voltage between the neighboring sensing
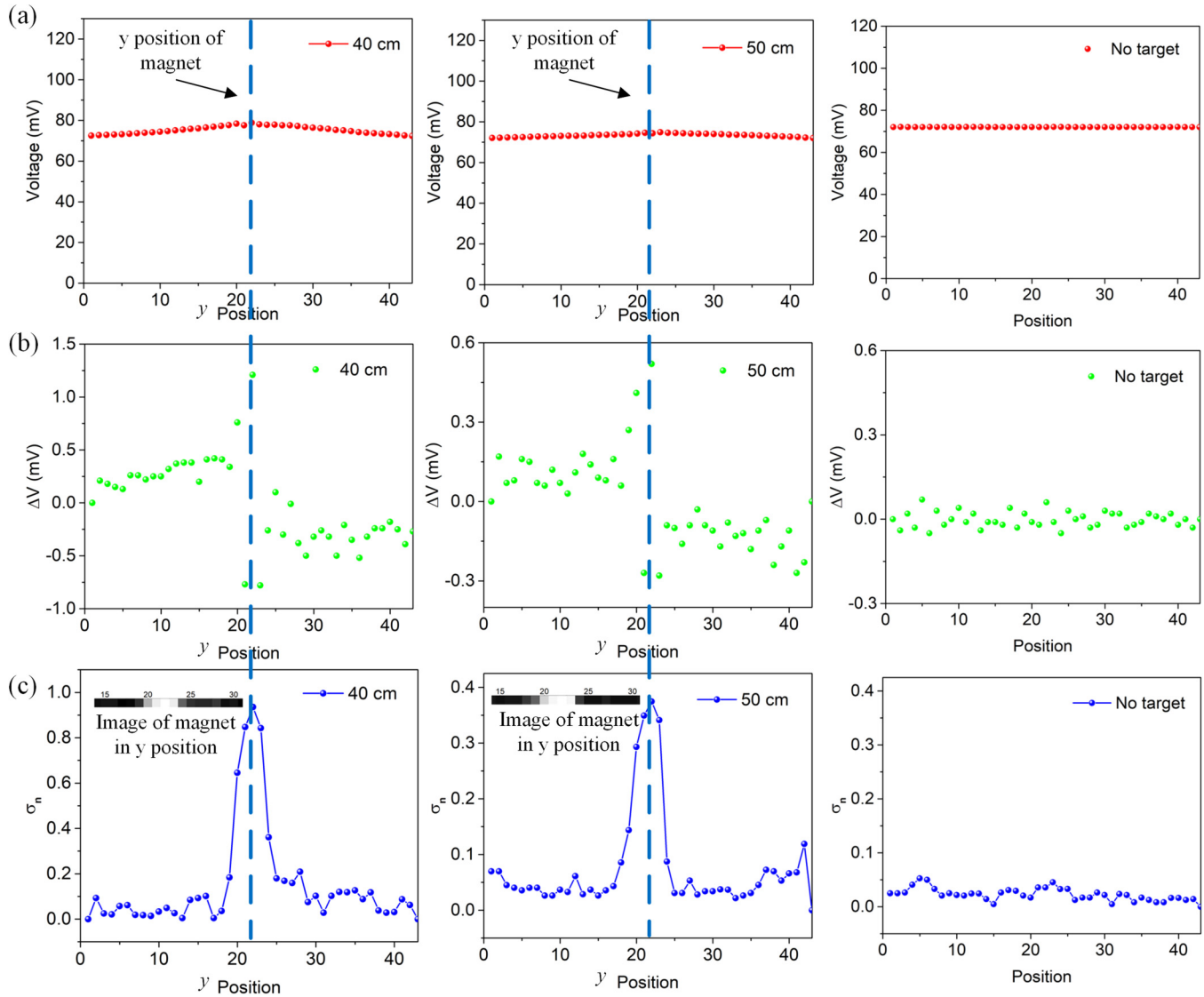
FIG. 5. (a) Measured output voltage from the sensing array when the magnet is placed at the (40, 22) and (50, 22) positions, compared to the scenario without a magnet target. (b) Calculated increment of the output voltage. (c) Calculated standard deviation of the signal and the image of the magnet (inset).

elements was calculated by $\Delta V_n = V_n - V_{n-1}$. Then, the standard deviation of ΔV can be calculated by

$$\sigma_n = \sqrt{D_n} = \sqrt{E[(x_n - \bar{x})^2]}, \qquad (4)$$

where x_n is the ΔV at position n and $\bar{x}$ is the mean value of ΔV, so the position of magnet target can be detected by confirming the maximum σ_n. The advantage of using maximum σ_n is that the intensity of the detected magnetic field has a minimal effect on the exact position of the magnet target.

Figure 5(a) displays the measured output voltage curve when the magnet is placed at the A (40, 22) and B (50, 22) positions, and comparing the scenario without a magnet target. Note that there is no change in the output voltage curve when the magnet target is absent in the sensing area. Some minor fluctuation in ΔV and σ_n can be neglected. However, a clear change in the ME output voltage from the sensors can be observed when the magnet source is placed in the sensing area. The output voltage curve indicates that the ME coupling output of the sensing array is impacted by both the magnetic field strength and the position of the magnet target. For the magnet at position A, the amplitude of the center

voltage is ~79 mV, while the peak output voltage is ~75 mV for position B. The difference between the two peak voltages is attributed to the difference in the weak DC magnetic field intensity being detected by the sensing array. The curves in Fig. 5(b) present the calculated ΔV, where the maximum ΔV is on the order of ~1.2 mV and 0.6 mV for the magnet located at positions A and B, respectively. ΔV consists of the contributions from the intensity of the magnetic field and the relative position between the sensor array and the magnet target. To acquire the accurate position of the magnet, the standard deviation of ΔV is calculated, as given in Fig. 5(c). As expected, the peak value of the standard deviation reflects the position of sensed magnet along the y axis. Clearly, the standard deviation curves can correctly represent the y position of the magnet, indicating the high sensing accuracy of the proposed sensing array, which can be easily recognized via the images shown in the insets.

The proposed sensing array is designed for one-dimensional (1D) magnetic field positioning; however, the sensing result can be misled by changing the direction of the magnetic field. To overcome this limitation, the sensing array can be improved by designing a multi-dimension array, which is capable of achieving 2D or 3D magnetic field positioning.

IV. CONCLUSION

In summary, the design, fabrication, and experimental measurements of a magnetic field ME sensor utilizing a laminated face shear mode PMN–PT/Metglas were reported. Weak AC/DC magnetic fields, being on the order of 2×10^{-8} Oe (AC) and 2×10^{-6} Oe (DC), can be detected. A 1D sensor array was also proposed for sensing the position of a weak magnetic field of 2×10^{-6} Oe, which demonstrates its great potential for weak magnetic field sensing and positioning.

ACKNOWLEDGMENTS

DATA AVAILABILITY

The data that support the findings of this study are available on request from the corresponding author. The data are not publicly available due to privacy or ethical reasons.

REFERENCES

[1]R. Jahns, R. Knöchel, H. Greve, E. Woltermann, E. Lage, and E. Quandt, in *IEEE International Symposium on Medical Measurements and Applications* (IEEE, Bari, 2011), p. 107.

[2]H. Lin, M. Zaeimbashi, N. Sun, X. Liang, H. Chen, C. Dong, A. Matyushov, X. Wang, Y. Guo, Y. Gao, and N.-X. Sun, in *IEEE International Microwave Biomedical Conference (IMBioC)* (IEEE, Philadelphia, PA, 2018), p. 13.

[3]Y. J. Wang, J. Q. Gao, M. H. Li, Y. Shen, D. Hasanyan, J. F. Li, and D. Viehland, Philos. Trans. R. Soc. A **372**, 20120455 (2014).

[4]Z. Chu, M. PourhosseiniAsl, and S. Dong, J. Phys. D Appl. Phys. **51**, 243001 (2018).

[5]A. V. Turutin, J. V. Vidal, I. V. Kubasov, A. M. Kislyuk, M. D. Malinkovich, Y. N. Parkhomenko, S. P. Kobeleva, O. V. Pakhomov, A. L. Kholkin, and N. A. Sobolev, Appl. Phys. Lett. **112**, 262906 (2018).

[6]M. Li, A. Matyushov, C. Dong, H. Chen, H. Lin, T. Nan, Z. Qian, M. Rinaldi, Y. Lin, and N. X. Sun, Appl. Phys. Lett. **110**, 143510 (2017).

[7]See https://www.lakeshore.com/products/categories/overview/magnetic-products/gaussmeters-teslameters/model-475-dsp-gaussmeter for the information of the sensitivity of a commercial gaussmeter.

[8]G. Liu, W. Jiang, J. Zhu, and W. Cao, Appl. Phys. Lett. **99**, 162901 (2011).

[9]S. Zhang and T. R. Shrout, IEEE Trans. Ultrason. Eng. **57**, 2138 (2010).

[10]Z. Chu, H. Shi, W. Shi, G. Liu, J. Wu, J. Yang, and S. Dong, Adv. Mater. **29**, 1606022 (2017).

[11]J. Gao, D. Gray, Y. Shen, J. Li, and D. Viehland, J. Appl. Phys. **99**, 153502 (2011).

[12]F. Li, S. Zhang, Z. Xu, X. Wei, and T. R. Shrout, Adv. Funct. Mater. **21**, 2118 (2011).

[13]X. Jiang, J. Kim, and K. Kim, Crystals **4**, 351 (2014).

[14]Y. Wang, P. Finkel, J. Li, and D. Viehland, J. Appl. Phys. **113**, 172904 (2013).

[15]S. Zhang, W. Jiang, R. J. Meyer, Jr., F. Li, J. Luo, and W. Cao, J. Appl. Phys. **110**, 064106 (2011).

[16]S. Zhang, F. Li, W. Jiang, J. Luo, R. J. Meyer, Jr., W. Cao, and T. R. Shrout, Appl. Phys. Lett. **98**, 182903 (2011).

[17]P. Berik, W. Y. Chang, and X. Jiang, Proc. SPIE **10598**, 105981F (2018).

[18]K. Kim, S. Zhang, and X. Jiang, IEEE Trans. Ultrason. Eng. **59**, 2548 (2012).

[19]S. Li, W. Jiang, L. Zheng, and W. Cao, Appl. Phys. Lett. **102**, 183512 (2013).

[20]Z. Chen, X. Li, P. Ci, G. Liu, and S. Dong, Rev. Sci. Instrum. **86**, 035002 (2015).

[21]X. Shi, W. Huang, F. Li, Z. Li, Z. Xu, X. Jiang, and X. Wei, AIP Adv. **6**, 115017 (2016).

[22]S. Park, M. Peddigari, G.-T. Hwang, W.-H. Yoon, A. Kumar, and J. Ryu, Appl. Phys. Lett. **115**, 102901 (2019).

[23]J. Ryu, A. V. Carazo, K. Uchino, and H.-E. Kim, Jpn. J. Appl. Phys. **40**, 4948 (2001).

[24]J. Ryu, S. Priya, K. Uchino, and H.-E. Kim, J. Electroceram. **8**, 107 (2002).

[25]I. M. Daniel and O. lshai, *Engineering Mechanics of Composite Materials* (Oxford University Press, New York, 1994), Vol. 3.

[26]J. V. Vidal, A. V. Turutin, I. V. Kubasov, M. D. Malinkovich, Y. N. Parkhomenko, S. P. Kobeleva, A. L. Kholkin, and N. A. Sobolev, IEEE Trans. Ultrason. Eng. **64**, 1102 (2017).

[27]L. Yana, Z. Xing, Z. Wang, T. Wang, G. Lei, J. Li, and D. Viehland, Appl. Phys. Lett. **94**, 192902 (2009).

[28]C. Fang, J. Jiao, J. Ma, D. Lin, H. Xu, X. Zhao, and H. Luo, J. Phys. D Appl. Phys. **48**, 465002 (2015).

[29]V. Annapureddy, H. Palneedi, W.-H. Yoon, D.-S. Park, J.-J. Choi, B.-D. Hahn, C.-W. Ahn, J.-W. Kim, D.-Y. Jeong, and J. Ryu, Sens. Actuators A **260**, 206 (2017).

[30]C. W. Nan, Phys. Rev. B **50**, 6082 (1994).

[31]C. W. Nan, M. Li, and J. H. Huang, Phys. Rev. B **63**, 144415 (2001).

[32]C. W. Nan, G. Liu, and Y. Lin, Appl. Phys. Lett. **83**, 4366 (2003).

[33]C. W. Nan, M. I. Bichurin, S. Dong, D. Viehland, and G. Srinivasan, J. Appl. Phys. **103**, 191–293 (2008).

[34]D. A. Pan, Y. Bai, W. Y. Chu, and L. J. Qiao, J. Phys. Condens. Matter **20**, 025203 (2008).

[35]G. T. Hwang, H. Palneedi, B. M. Jung, S. J. Kwon, M. Peddigari, Y. Min, J. W. Kim, C. W. Ahn, J. J. Choi, B. D. Hahn, J. H. Choi, W. H. Yoon, D. S. Park, S. B. Lee, Y. Choe, K. H. Kim, and J. Ryu, ACS Appl. Mater. Interfaces **10**, 32323 (2018).

[36]S. Goljahi, J. Gallagher, S. J. Zhang, J. Luo, R. Sahul, W. Hackenberger, and C. S. Lynch, Smart Mater. Struct. **21**, 055005 (2012).

[37]Y. Shen, D. Hasanyan, J. Gao, Y. Wang, J. Li, and D. Viehland, Smart Mater. Struct. **22**, 095007 (2013).

[38]Y. Shen, J. Wang, J. Shi, S. Zhao, and J. Gao, J. Magn. Magn. Mater. **484**, 164 (2019).

[39]Y. Shen, K. L. McLaughlin, J. Gao, D. Gray, L. Shen, Y. Wang, M. Li, D. Berry, J. Li, and D. Viehland, Smart Mater. Struct. **21**, 065007 (2012).

[40]Z. Chu, W. Shi, H. Shi, Q. Chen, L. Wang, M. J. PourhosseiniAsl, C. Xiao, T. Xie, and S. Dong, Adv. Mater. Technol. **4**, 1800484 (2018).